Synchronization of a Van Der Pol Oscillator to a Two-Frequency Signal

Aaron Daniel

Supervisor: M. Koppenhöfer

February 11, 2020

Contents

Introduction

Oscillations are abundant in our universe and their description forms a crucial part of our understanding of this worlds working mechanisms. From sound-waves to the tide, from the beating of a human heart to the undulatory description of the microscopic world, oscillation is an omnipresent pattern on many scales.

One subclass of the many oscillators that exist are self-sustained oscillators. They form a particularly interesting case where the oscillations are driven by an internal energy supply of the system that exhibits them. Among them are for example the flashing of fireflies, the beating of a heart, the motion of a metronome or the oscillations of a pendulum clock. Regardless of their initial state or a nonrecurring external perturbation, these oscillations always return to the same rhythm and continue to oscillate. The defining features of these systems are the stability in regard to their amplitude and the controllability of their phase. This means perturbations to the amplitude decay quickly and perturbations to the phase do not decay at all. Mathematically what all these systems have in common is the feature of a stable and attractive limit cycle in their phase space, an asymptotically stable amplitude and a neutrally stable phase.

It was in 1655 that Christiaan Huygens first observed an intriguing feature of self-sustained oscillators. Suspending two pendulum clocks from a wooden beam, he observed that after some time the two clocks adjusted their frequencies to oscillate in unison and thereby made one of the first observations of the phenomenon refered to as synchronization. This phenomenon, that self-sustained oscillators if affected continuosly by an external periodic force can adjust their own rhythm, has now been intensively studied, has had many applications in diverse fields and will also be the topic of discussion in this report.

While numerous books and articles exist on the synchronization properties of systems exhibiting self-sustained oscillations with a single-frequency signal, the question of how a self-sustained oscillator responds to a multi-frequency signal has received little attention.

In this report we investigate the synchronization properties of the van der Pol oscillator, a paradigmatic self-sustained oscillator, when subjected to two periodic signals of different frequency. Derived in 1920 in the context of his work at Philips by Balthazar van der Pol the van der Pol equation has been used to model many oscillatory processes in diverse fields of the natural sciences and has established itself as an exemplary self-sustained oscillator.

Starting from the theory and analytical methods developed to analyze synchronization of self-sustained oscillators to a single periodic signal, we will try to extend these methods to the case of two signals and use numerical simulations to advance into selected areas of the parameter space.

Chapter 1

Theoretical Background

In this chapter we briefly consider the limit cycle of the van der Pol oscillator, describe the theoretical approach to synchronization to a single-frequency signal and detail the knowledge on synchronization to a two-frequency signal. Lastly we will touch on numerical methods used in our investigation.

1.1 Limit cycle of the van der Pol oscillator

The van der Pol oscillator is described by the following equation of motion:

$$\ddot{u} + \omega_0^2 u - 2\epsilon\dot{u}\left(1 - \beta u^2\right) = 0 \ . \tag{1.1}$$

Here $u(t)$ is the position, ω_0 is the natural frequency and β,ϵ are two parameters. The equation consists of the first two terms making up a harmonic oscillator and a third term which, dependent on the amplitude, describes positive or negative damping. This feature of an amplitude-dependent damping makes the homogeneous van der Pol equation a classical example of a limit-cycle oscillator. Given any nonzero random initial condition, after a time of transient dynamics the oscillator will end up on the same circular trajectory in phase space called a limit cycle. This behaviour is illustrated in Fig. 1.1. Along this limit cycle the trajectory is neutrally stable, meaning perturbations do not decay, whereas transversal to the limit cycle the trajectory is asymptotically stable, meaning perturbations decay and the trajectory returns to the limit cycle. [1]
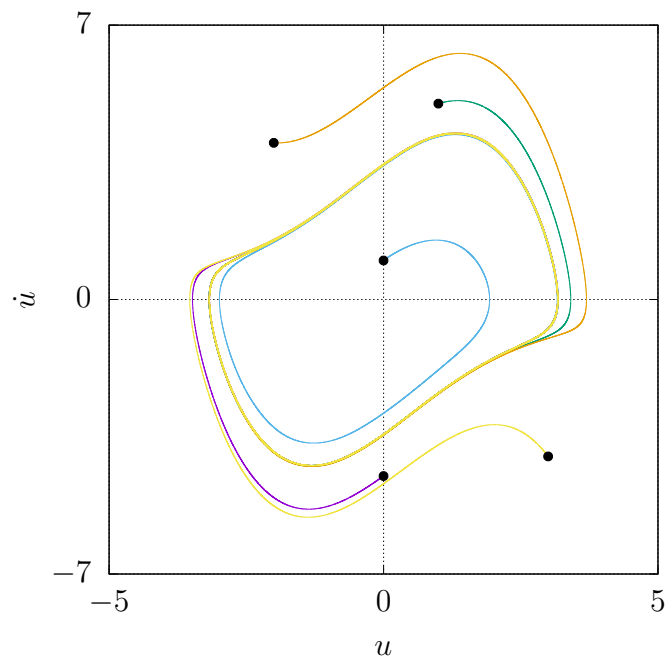
Figure 1.1: Trajectories of a van der Pol oscillator in phase space for different initial conditions (black dots) all result in the same limit cycle. Parameters: $\epsilon = 0.5$, $\beta = 0.4$ and $\omega_0 = 1$.

1.2 Van der Pol oscillator with single-frequency signal

To understand the methods to deal with synchronization and to get an idea of the possible dynamics, we now consider the van der Pol oscillator driven by a single-frequency signal

$$\ddot{u} + \omega_0^2 u - 2\epsilon\dot{u}\left(1 - \beta u^2\right) = K\cos(\omega t) \ . \tag{1.2}$$

In the following we review the general procedure to deal with a self-sustained oscillators subjected to a periodic signal detailed in [1] and apply it to our differential equation.

In this case we expect synchronization to the external signal and are therefore interested in solutions oscillating at the frequency of the external drive signal ω. We make the ansatz,

$$u(t) = \frac{1}{2}A(t)e^{i\omega t} + c.c. \ . \tag{1.3}$$

Here we take the complex amplitude A as a slowly varying correction to the amplitude and frequency of the signal and therefore introduce the relation:

$$\dot{u}(t) = \frac{1}{2}A(t)i\omega e^{i\omega t} + c.c. \ . \tag{1.4}$$

We use a two-timing approach. For a more detailed derivation of this see [2]. Plugging Eqs. (1.3) and (1.4) into Eq. (1.2), we get a differential equation for the complex amplitude A,

$$\dot{A} = \frac{e^{-i\omega t}}{i\omega}\left[(\omega^2 - \omega_0^2)u + 2\epsilon\dot{u}(1 - \beta u^2) + K\cos(\omega t)\right] \ . \tag{1.5}$$

We now restrict ourselves to large and slow variations of the amplitude and therefore neglect all rapidly oscillating terms on the right hand side (r.h.s) of Eq. (1.5). This procedure is called averaging and leads us to an approximation for the complex amplitude equation,

$$\dot{A} = -i\frac{\omega^2 - \omega_0^2}{2\omega}A + \epsilon A - \frac{\epsilon\beta}{4}|A|^2 A - \frac{iK}{2\omega} + O(\epsilon^2) \ . \tag{1.6}$$

We now make the following substitutions

$$A = \frac{2}{\sqrt{\beta}}a, \quad t = \frac{\tau}{\epsilon}, \quad \nu = \frac{\omega^2 - \omega_0^2}{2\omega\epsilon}, \quad e = \frac{K\sqrt{\beta}}{4\omega\epsilon} \ ,$$
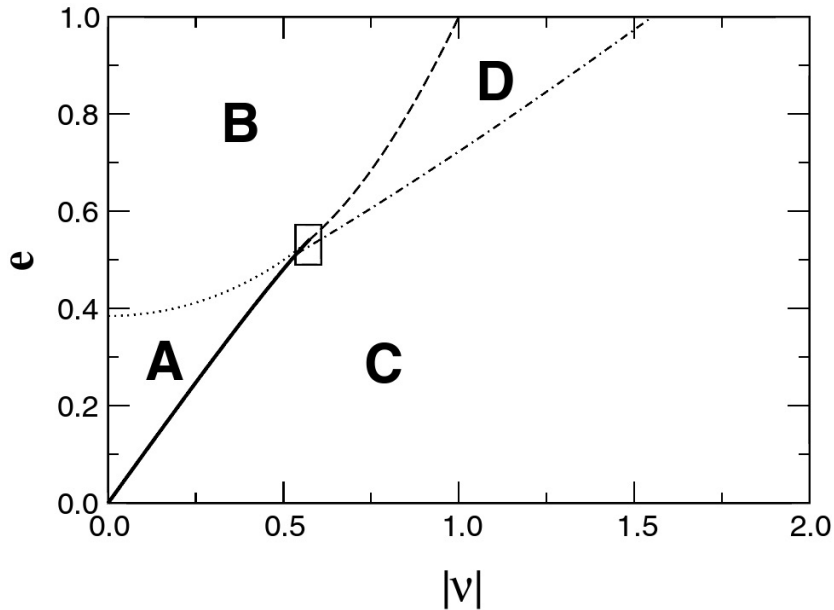
Figure 1.2: Bifurcation diagram for the isochronous forced weakly nonlinear oscillator from [3].

where a is the amplitude normalized to the natural amplitude, τ the dimensionless time, ν the dimensionless detuning and e the dimensionless drive strength. This yields our final differential equation for the normalized complex amplitude

$$\dot{a} = -i\nu a + a - |a|^2 a - ie \ . \tag{1.7}$$

We now consider the fixed points and limit cycles of this differential equation to get an understanding of the resulting motion for different values of the drive strenght and the detuning. As Eq. (1.7) is generally valid for isochronous weakly forced nonlinear oscillators, we adopt the classification from [1] as it stands.

Depending on the detuning ν and the normalized drive strenght e one can indentify four major regions in the bifurcation diagram of (1.7), shown in Fig. 1.2:

Region A For small drive strength and small detuning, two fixed points exist of which one is stable and one is unstable. After a transient time, A takes a fixed value and the oscillator therefore synchronizes to the frequency of the external drive with a constant phase shift. Example trajectories can be seen in Fig. 1.3a.

Region B For small detuning and moderate drive strength, only one stable fixed point exists. The oscillator still synchronizes to the frequency of

the external drive with a constant phase shift. Example trajectories can be seen in Fig. 1.3b.

Region D For moderate drive strength and detuning, a stable limit cycle exists which does not envelop the origin. Thus, A is no longer constant but has a fixed and finite average phase and the oscillation therefore synchronizes to the frequency of the external drive as the additional rotation in the rotating frame is zero on average. Example trajectories can be seen in Fig. 1.3d.

Region C For large detuning, a stable limit cycle exists which envelops the origin. The frequency of the oscillation is ω plus the rotation of A and the resulting motion is quasiperiodic and asynchronous to the frequency of the external drive signal. Example trajectories can be seen in Fig. 1.3c.

The box around the meeting point of all regions in Fig. 1.3 contains complex bifurcations which we will not explain here. For a mored detailed discussion see [4].
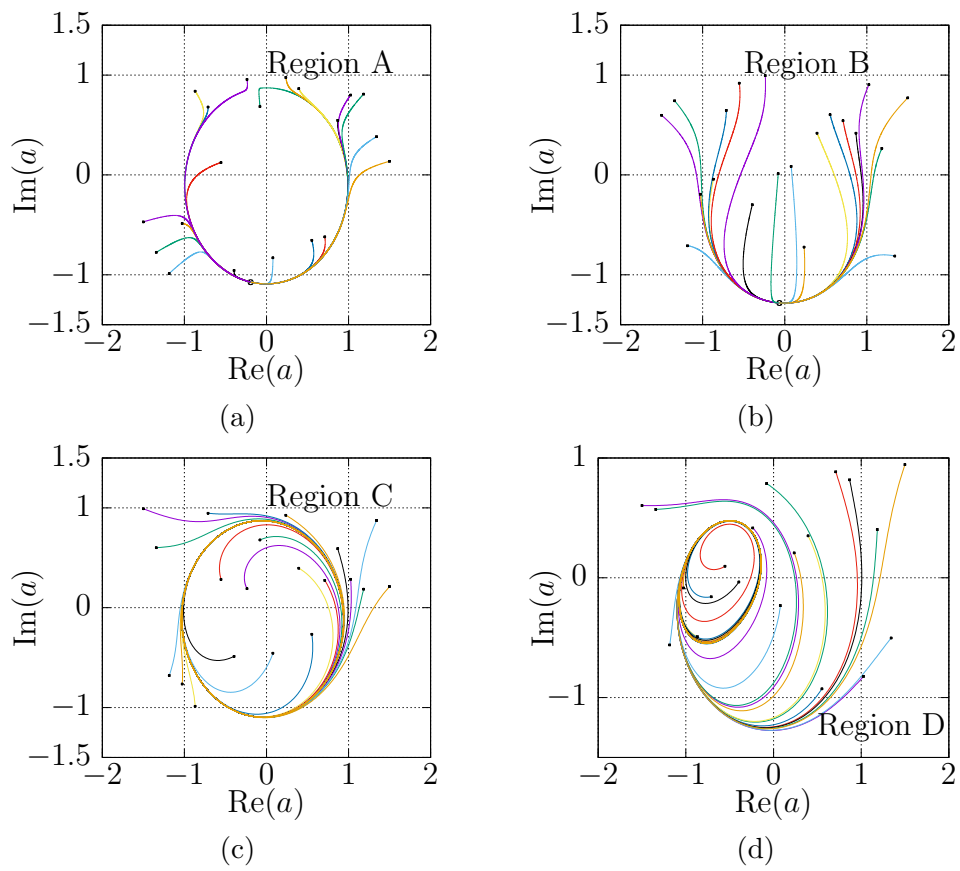
Figure 1.3: Trajectories of the amplitude a in the complex plane for the different regions of the bifurcation diagram in Fig. 1.2.

1.3 The circle map and response to a two-frequency signal

To describe the synchronization behaviour of a self-sustained oscillator subject to a two-frequency drive signal we need to introduce the concept of the circle map. In this explanation we will again closely follow the treatment of the theory in [1].

Because we know the dynamics of a self-sustained oscillator in the homogeneous case, we can describe the dynamics of the system subjected to a periodic forcing by continuity arguments. As the homogeneous case leads to a limit cycle in phase space, the dynamics in its vicinity evolve inside a ring around that limit cycle. For a small amplitude of the external drive signal, these dynamics have an attractive and invariant curve which is described by the circle map [1]. In this case of a weak signal, the dynamics of the amplitude can be neglected as it is asymptotically stable and we can investigate the main properties of the system close to the limit cycle by focusing on the phase equation

$$\dot{\phi} = \omega_0 + K \cdot Q(\phi, t) \ , \tag{1.8}$$

where ω_0 is again the natural frequency of the system, K is the amplitude of the external signal, and ϕ is the phase of the resulting motion in phase space. The function $Q(\phi, t)$ is 2π-periodic in ϕ and T-periodic in t. Its exact form depends on the structure of the signal and the oscillator in question.

In the case of a single-frequency signal, the phase space of this equation is a 2D-torus that can be reduced to a one-dimensional mapping by taking a stroboscopic view with time interval T. This maps $\phi_n(t)$ to $\phi_{n+1}(t + T)$. Choosing an arbitrary initial time t_0 we construct a smooth invertible circle map,

$$\phi_{n+1} \equiv \phi_n + \omega_0 T + \epsilon F(\phi_n) \qquad \mod 2\pi \ . \tag{1.9}$$

The function $F(\phi)$ again depends on the structure of the signal and the oscillator. This stroboscopic view on the trajectories in phase space allows us to distinguish between synchronized or nonsynchronized motion resulting from an external signal. For an invertible circle map, we characterize the dynamics with the rotation number that gives the average phase shift per one iteration,

$$\rho(\phi_0) = \lim_{n \to \infty} \frac{\phi_n - \phi_0}{2\pi n} \ . \tag{1.10}$$

The rotation number ρ does not depend on the initial value ϕ_0 nor on the direction of the limit $n \to \infty$ or $n \to -\infty$ [1]. Because the number of iterations n can be rewritten as the elapsed time divided by the time-interval of the stroboscopic mapping $\frac{t}{T}$, we can derive that the rotation number is
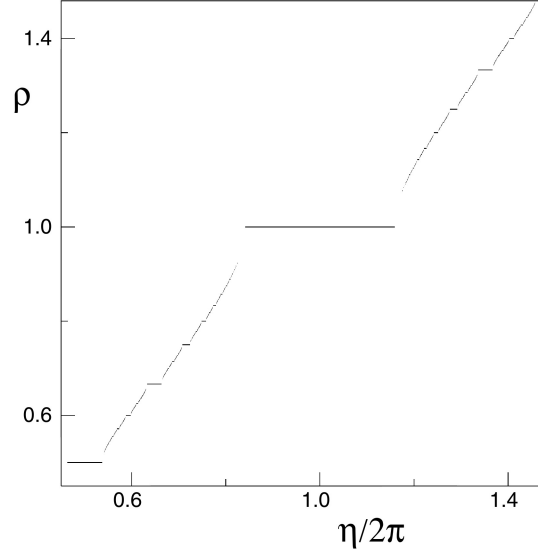
Figure 1.4: Rotation number ρ as a function of parameter $\eta = \omega_0 T$ for the sine circle map from [1].

the ratio between the observed frequency Ω and the frequency of the drive signal ω,

$$\rho = \lim_{t \to \infty} \frac{T \cdot (\phi_n - \phi_0)}{2\pi t} = \frac{\Omega}{\omega} \ , \tag{1.11}$$

with Ω being the average velocity of the phase,

$$\Omega = \lim_{t \to \infty} \frac{\phi(t) - \phi_0}{t} \ . \tag{1.12}$$

From this we can conclude that a rational rotation number corresponds to synchronized motion (motion with the frequency of the drive signal or in rational relation to this frequency) and an irrational rotation number to nonsynchronous motion. Further analysis shows that synchronization does occur for all rational combinations,

$$\rho = \frac{p}{q} \ ,$$

where the width of the synchronization regions in the plane of detuning and drive strength decreases with q [1]. For a fixed drive strength the rotation number is a Cantor function or Devil's Staircase, as illustrated in Fig. 1.4. If the signal contains two frequencies, the phase equation takes the form

$$\dot{\phi} = \omega_0 + K \cdot Q(\phi, \omega_1 t, \omega_2 t) \ , \tag{1.13}$$

11

where ω_1 and ω_2 are the two frequencies contained in the signal. This equation now describes the motion on a three-dimensional torus. Again a circle map can be derived and the rotation number exists. It can be shown that in this case the phase of the system is locked if the observed frequency is a rational combination of the two signal frequencies,

$$\rho = \frac{p_2}{q_2}\frac{\omega_2}{\omega_1} + \frac{p_1}{q_1} \tag{1.14}$$

otherwise, the system is not synchronized. [5, 1]

1.4 Noise and stochastic differential equations

Any realization of a self-sustained oscillator in the real world will be subject to some sort of noise. Be it thermal noise, shot noise, or any other kind of environmental noise, small stochastic perturbations will always be present and it is of interest to know whether the results found in the noise-free case persist in the presence of noise. To determine this we will add a Gaussian white-noise term to our signal and numerically solve the differential equations for several regions of the parameter space. Noise is a stochastic process and leads to a stochastic differential equation which will have a stochastic process as a solution. We will shortly introduce the basic theory and necessary notation.
Starting from a general first order differential equation,

$$\frac{dx}{dt} = a(x,t) \ , \tag{1.15}$$

we obtain a stochastic differential equation by adding a time-dependent noise term $\chi(t)$ with a prefactor $b(x,t)$,

$$\frac{dx}{dt} = a(x,t) + b(x,t)\chi(t) \ . \tag{1.16}$$

This can be rewritten by formal integration over infinitesimal dt,

$$x(t) = x(t_0) + \int_{t_0}^{t} dt' a[x(t'),t'] + \int_{t_0}^{t} dW(t')b[x(t'),t'], \tag{1.17}$$

a short hand notation:

$$dx(t,\omega) = a[x(t),t]dt + b[x(t),t]dW(t) \ , \tag{1.18}$$

see ref. [6].

1.5 Numerical methods

The calculations done for this project were all carried out in the programming language *Julia*. Here we want to quickly touch on our method of determining the observed frequency ω_{obs} and a crucial software package used during the numerical investigation.

1.5.1 Solving the differential equations

To solve the differential equations we used the *DifferentialEquations.jl* package in Julia [7]. For detailed information on the package we refer the interested reader to the cited paper. During our calculations we used the Tsitouras 5 Runge-Kutta method for the ordinary differential equations and the implicit Runge-Kutta discretization of the 1.0 Milstein method for the stochastic differential equations, and a relative tolerance of 10^{-6}.

1.5.2 Determining the observed frequency

To infer the observed frequency ω_{obs} from the numerical solution of the differential equation, we proceed as follows: The phase of the numerical solution is extracted by calculating the inverse tangent of the first derivative of the amplitude and the amplitude. See Fig. 1.5 for an example. To perform an adequate fit and get the frequency we unwrap the phase, thereby changing the formerly 2π-periodic signal to an injective function. On this data we then perform a linear fit whose slope yields the observed frequency ω_{obs}.
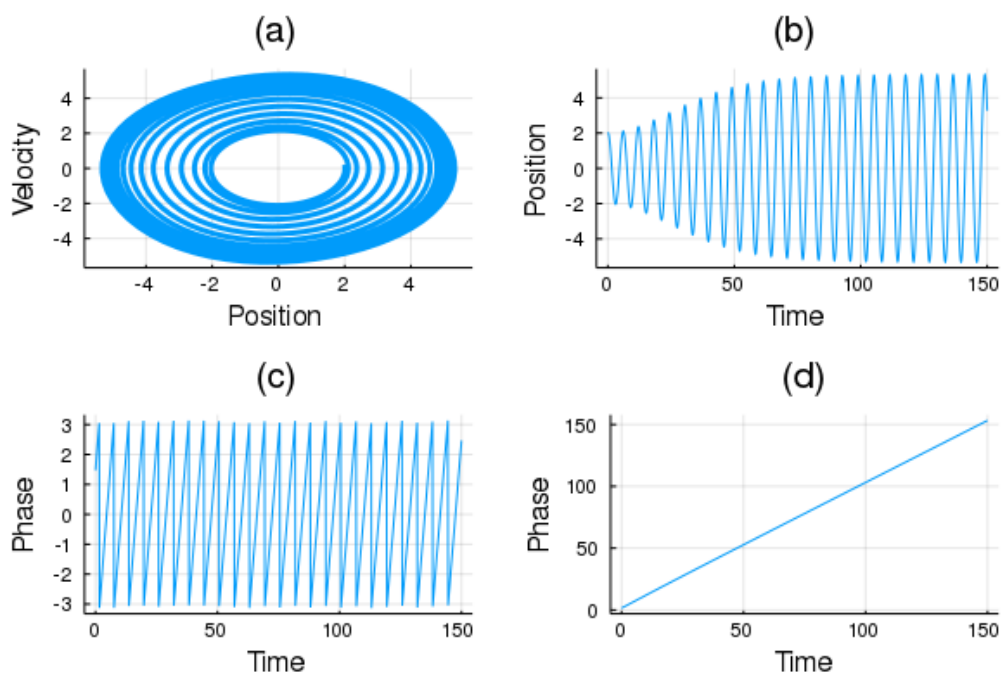
Figure 1.5: (a) Trajectory of the solution in phase space. (b) Position in real space as a function of time. (c) Extracted phase ϕ as a 2π-periodic function. (d) Unwrapped phase ϕ.

Chapter 2

Analytical Results

In this chapter we will present the analytical approach we took to the problem of a van der Pol oscillator subject to a two-frequency signal by applying a two-timing approach.

2.1 Van der Pol oscillator with a two-frequency signal

In this investigation we closely follow the procedures done in Ref. [8] for similar problems. To investigate the case of a weak signal, we take the drive to be proportional to ϵ,

$$\ddot{u} + \omega_0^2 u - 2\epsilon\dot{u}\left(1 - \beta u^2\right) = \epsilon E(t) , \tag{2.1}$$

where now the drive consists of a signal with two frequencies,

$$E(t) = K_1 \cos\left(\Omega_1 t + \theta_1\right) + K_2 \cos\left(\Omega_2 t + \theta_2\right) . \tag{2.2}$$

To get an approximate solution, we use a two-timing approach, for detailed explanation see [2],

$$u(t; \epsilon) = u_0(T_0, T_1) + \epsilon\, u_1(T_0, T_1) + O(\epsilon^2) . \tag{2.3}$$

We adapt the notation of [8] and define:

$$T_0 = t \quad T_1 = \epsilon\, t$$

$$D_0 := \frac{\partial}{\partial T_0} \quad D_1 := \frac{\partial}{\partial T_1} .$$

By plugging the approach into Eq. (2.1) and comparing coefficients of ϵ, we get two differential equations,

$$D_0^2 u_0 + \omega_0^2 u_0 = 0 , \tag{2.4}$$

$$D_0^2 u_1 + \omega_0^2 u_1 = 2\left(D_0 u_0 - \beta u_0^2 D_0 u_0 - D_1 D_0 u_0\right) + E(T_0) . \tag{2.5}$$

Equation (2.4) can easily be solved by

$$u_0 = A(T_1)e^{i\omega_0 T_0} + c.c. \tag{2.6}$$

Now we rewrite the drive frequencies as follows to show the detunings σ_1, σ_2 with respect to the natural frequency ω_0,

$$\Omega_1 := \omega_0 + \epsilon\sigma_1 \quad \Omega_2 := \omega_0 + \epsilon\sigma_2 .$$

Therefore the drive becomes:

$$E(T_0) = \frac{K_1}{2}e^{i(\omega_0 T_0 + \sigma_1 T_1 + \theta_1)} + \frac{K_2}{2}e^{i(\omega_0 T_0 + \sigma_2 T_1 + \theta_2)} + c.c. . \tag{2.7}$$

Equation (2.5) can be rewritten as:

$$D_0^2 u_1 + \omega_0^2 u_1 =$$
$$\left[2i\omega_0 A - 2A'i\omega_0 - 2\beta i\omega_0 A|A|^2 + \frac{K_1}{2}e^{i(\sigma_1 T_1 + \theta_1)} + \frac{K_2}{2}e^{i(\sigma_2 T_1 + \theta_2)}\right]e^{i\omega_0 T_0}$$
$$- 2\beta A^3 e^{3i\omega_0 T_0} + c.c. . \tag{2.8}$$

We make an ansatz for $A(T_1)$:

$$A(T_1) = a(T_1) \cdot e^{i(\sigma T_1 + c(T_1))} := ae^{i(\sigma T_1 + c)} ,$$

where the amplitude $a(T_1)$, the phase $c(T_1)$ and an additional constant σ are all real variables. In order for the secular terms to vanish in Eq. (2.8) the following condition has to hold:

$$2ai\omega_0 e^{ic} - 2\beta i\omega_0 a'e^{ic} - 2i\omega_0 ae^{ic}(\sigma + c')$$
$$- 2\beta i\omega_0 ae^{ic}a^2 + \frac{K_1}{2}e^{i(\sigma_1 T_1 + \theta_1 - \sigma T_1)} + \frac{K_2}{2}e^{i(\sigma_2 T_1 + \theta_2 - \sigma T_1)} = 0 . \tag{2.9}$$

By splitting into real and imaginary part and rearranging we get two differential equations,

$$a(\sigma + c') = -\frac{K_1}{4\omega_0}\cos(\sigma_1 T_1 + \theta_1 - \sigma T_1 - c)$$
$$-\frac{K_2}{4\omega_0}\cos(\sigma_2 T_1 + \theta_2 - \sigma T_1 - c) \tag{2.10}$$

$$a' = \frac{K_1}{4\omega_0}\sin(\sigma_1 T_1 + \theta_1 - \sigma T_1 - c)$$
$$+\frac{K_2}{4\omega_0}\sin(\sigma_2 T_1 + \theta_2 - \sigma T_1 - c) - \beta a^3 + a \ . \tag{2.11}$$

We define the following variable:

$$\gamma_i := \sigma_i T_1 + \theta_i - \sigma T_1 - c \quad i = 1, 2 \ .$$

Rearranging again, we obtain

$$c' = -\frac{K_1}{4\omega_0 a}\cos(\gamma_1) - \frac{K_2}{4\omega_0 a}\cos(\gamma_2) - \sigma \tag{2.12}$$

$$a' = \frac{K_1}{4\omega_0}\sin(\gamma_1) + \frac{K_2}{4\omega_0}\sin(\gamma_2) - \beta a^3 + a \ . \tag{2.13}$$

These two differential equations now allow us to analyze the trajectories of the complex amplitude in an adjustable rotating frame. By varying σ we can choose different ratios between the two frequencies ω_1 and ω_2 and analyze the synchronization behaviour numerically by solving Eq. (2.1).
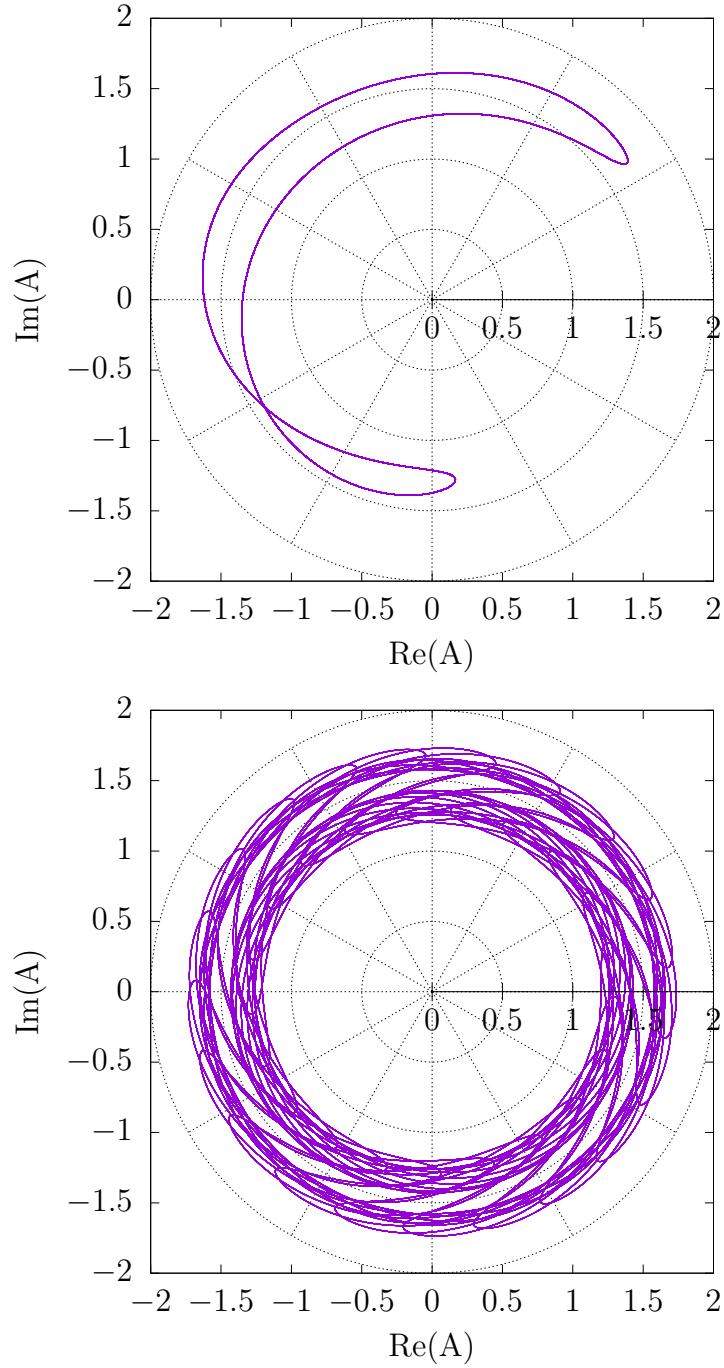
Figure 2.1: (a) Numerical solution for the parameters: $K_1 = K_2 = 2.0$, $\beta = 0.4$, $\omega_0 = 1.0$, $\sigma_1 = 0.54$, $\sigma_2 = 0.75$, $\theta_1 = \theta_2 = 0, \sigma = 2\sigma_1 - \sigma_2$ (b) numerical solution for the same parameters except $\sigma' = \sigma + 0.01$

Chapter 3

Numerical Results

In this chapter we will present the findings of the numerical simulations of the differential equation (2.1). We will discuss the observed frequency as a function of the signal frequencies and subsequently interpret our findings.

3.1 Noiseless simulation

3.1.1 Synchronization to a single-frequency signal

The synchronization region for the single-frequency case was first computed analytically using the theory discussed in Sec. 1.2. Synchronization is lost during the bifurcation at the transition from region A to region C in Fig. 1.2. With the parameters used in all numerical simulations here, the value for the frequency ω_{border} at which this bifurcation occurs can be calculated and amounts to $\omega_{\mathrm{border}} = 1.0032 \pm 0.0001$. We checked this result numerically by solving Eq. (1.2) for a range of signal frequencies, determining the observed frequency and checking whether the detuning $\omega_1 - \omega_{\mathrm{obs}}$ exceeded a value of 0.0001. The numerical result was: $\omega'_{\mathrm{border}} = 1.003183$ on a frequency resolution of $1.5 \cdot 10^{-6}$. The graph of this simulation can be seen in Fig. 3.1. In our further treatment we will use the analytically obtained value for the synchronization region in the single-frequency case. From now on we will refer to the region between the natural frequency $\omega_0 = 1$ and the border of the synchronization region $\omega_{\mathrm{border}} = 1.003200$ as the *synchronization region*.
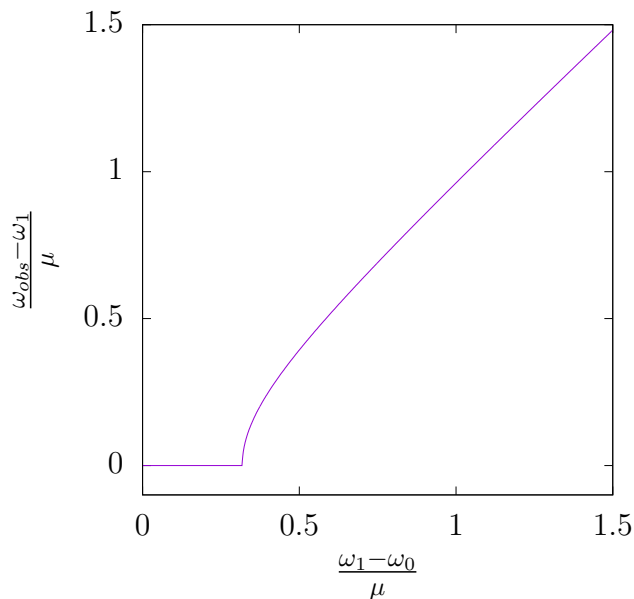
Figure 3.1: Entrainment plot for the single-frequency case

3.1.2 Synchronization to a two-frequency signal

Unless specified differently, in the following we solve the equation of the van der Pol oscillator subject to a two-frequency signal in the following form:

$$\ddot{u} + u - 2\epsilon\dot{u}\left(1 - \beta u^2\right) = \epsilon E(t) \ , \tag{3.1}$$

where we set for $\epsilon = 0.01$, $\beta = 0.4$ and the drive with $K_1 = K_2 = 2$:

$$E(t) = K_1 \cos\left(\omega_1 t\right) + K_2 \cos\left(\omega_2 t + \theta\right) \ . \tag{3.2}$$

The parameters were chosen such that we were able to investigate the following scenarios:

1. The frequencies of both signals are very close to each other. This should be equivalent to a single-frequency signal with an increased amplitude. This corresponds to the diagonal line in Fig. 3.2.

2. Both signal frequencies are in the synchronization region. This corresponds to region (a) in Fig. 3.2.

3. One frequency is in the synchronization region, the other frequency is outside the synchronization region. This corresponds to region (b) in Fig. 3.2.

4. Both signals are outside of the synchronization region. This corresponds to region (c) in Fig. 3.2.

As we expect the solution to oscillate close to the frequency of the signal for small signal strengths $\epsilon \ll 1$, and because we want to ensure having a reliable amount of data for extracting the observed frequency we adjusted the number of timesteps in our simulations to the signal. The signal can be rewritten as follows:

$$2\left[\cos\left(\omega_1 t\right) + \cos\left(\omega_2 t + \theta\right)\right] = 4\left[\cos\left(\frac{\omega_1 + \omega_2}{2}t\right)\cos\left(\frac{\omega_1 - \omega_2}{2}t + \theta\right)\right] ,$$
(3.3)

and has the period $T_{\text{sum}} = \frac{\pi}{|\omega_1 - \omega_2|}$. If the difference $|\omega_1 - \omega_2|$ decreases, the number of timesteps tends to infinity. To prevent this divergence a data point was not evaluated if the timesteps exceeded a given maximum value. We chose this method over using a fixed amount of timesteps to have the same accuracy for all the observed frequencies rather than having a decreasing accuracy for data points closer to the diagonal line. The effect of non-evaluated data points can be seen in Fig. 3.2 as the bright yellow area around the diagonal line. For details on solver algorithms, relative tolerance and software packages, see Sec. 1.5. As derived in Sec. 2.1, we expect the observed frequency in the synchronization region to be a rational combination of the two frequencies contained in the signal,

$$\omega_{\text{obs}} = q\omega_1 + p\omega_2 .$$
(3.4)

We calculated the gradient of the data visualized in Fig. 3.2 with respect to ω_1 and ω_2 to extract q and p. The results are illustrated in Figs. **??** and **??**. For details on the numerical derivative, see App. A.

Both signals in synchronization region

In the region of the (ω_1, ω_2)-plane where both signals are inside the synchronization region, we observe synchronization to rational combinations of the two frequencies. The combinations $(p, q) = (1, 0)$ and $(p, q) = (0, 1)$ are dominant except for a low detuning $|\omega_1 - \omega_2| \approx 0$ close to the diagonal. This is illustrated in Fig. 3.4.

One signal in synchronization region

If one signal is inside the synchronization region and the other signal is outside that region, we observe synchronization to the signal closer to the natural frequency. It is noteworthy that for decreasing detuning between the natural

21
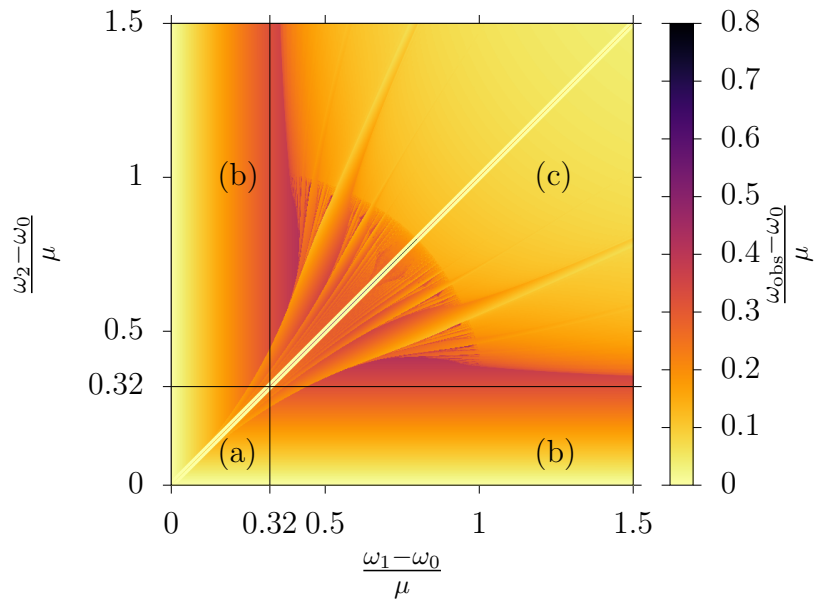
Figure 3.2: Observed frequency ω_{obs} as a function of both signal frequencies. Both frequencies have the same strength $K_1 = K_2 = 2$ and there is no phase shift between them, $\theta = 0$. (a) Both signals are inside the synchronization region, (b) one signal is inside the synchronization region and (c) no signal is inside the synchronization region.
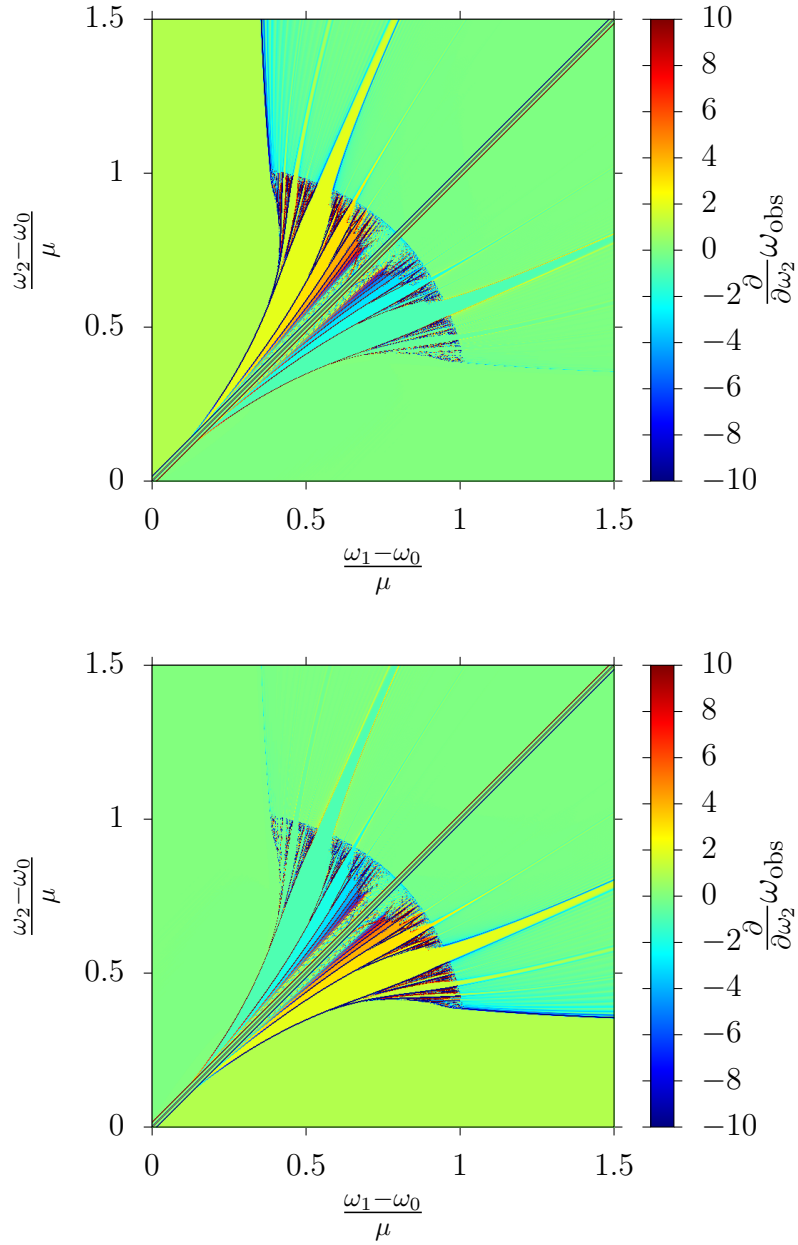
Figure 3.3: Upper graph shows the numerical derivative of the data visualized in Fig. 3.2 with respect to ω_1. Upper graph shows the numerical derivative of the data with respect to ω_2
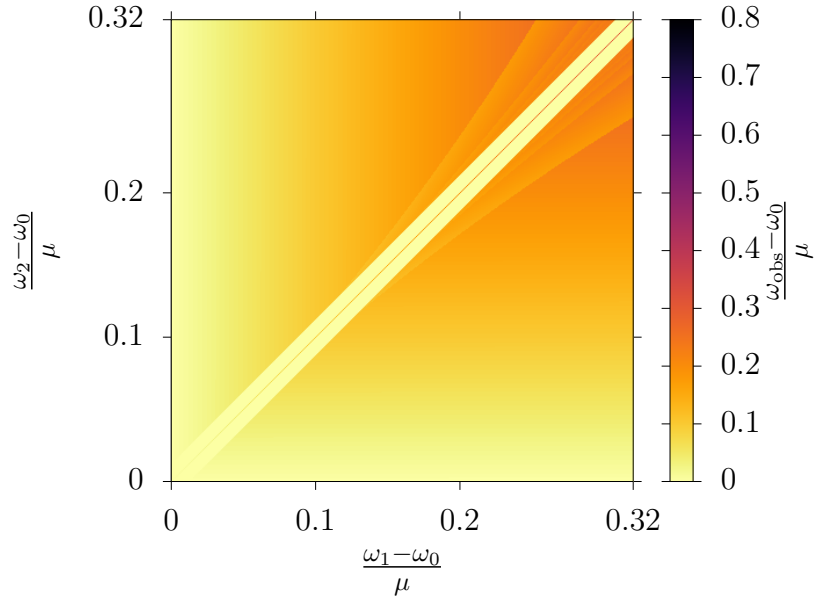
Figure 3.4: Both frequencies are inside the synchronization region. We observe synchronization to rational combinations of ω_1 and ω_2.

frequency and the second signal, the synchronization region increases in size. Specifically this means that the presence of a second signal with a different frequency amplifies synchronization to the first signal. This is illustrated in Fig. 3.5.

No signal in synchronization region

If both signals are outside of the synchronization region, we observe synchronization to rational combinations in a circle. The rational combinations are of the form:

$$\omega_{\mathrm{obs}} = q\omega_1 + p\omega_2 \ . \tag{3.5}$$

For increasing absolute values of q and p the synchronization regions decrease in size and extend less far into the (ω_1, ω_2)-plane. Along the diagonal line where the frequency of both signals coincides, we observe synchronization to the common frequency. Note that the region directly around the diagonal line could not be resolved due to technical restrictions described earlier. This is illustrated in Fig. 3.6.
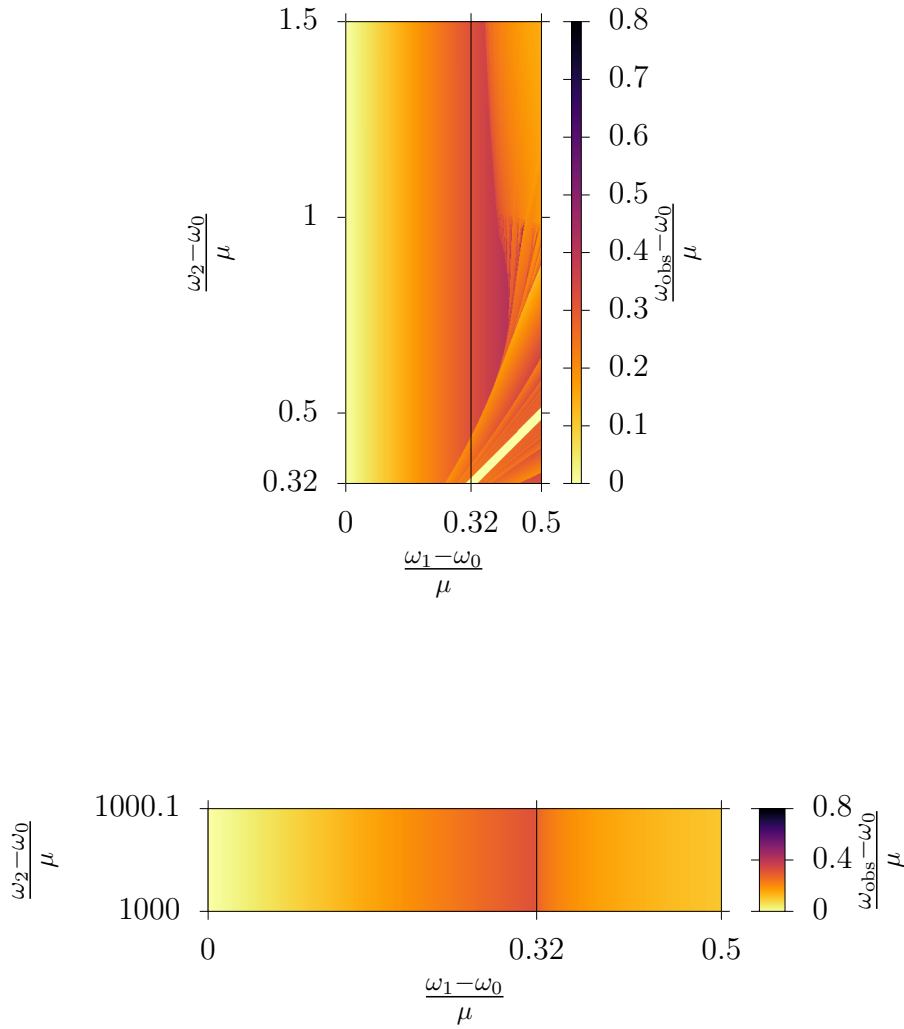
Figure 3.5: Upper graph shows a focus on the region where the signal K_1 is inside the synchronization region and signal K_2 is outside this region. We observe synchronization to the signal closer to the natural frequency ω_0. The synchronization region is shown by the black line. Lower graph shows a horizontal cut for large ω_2.
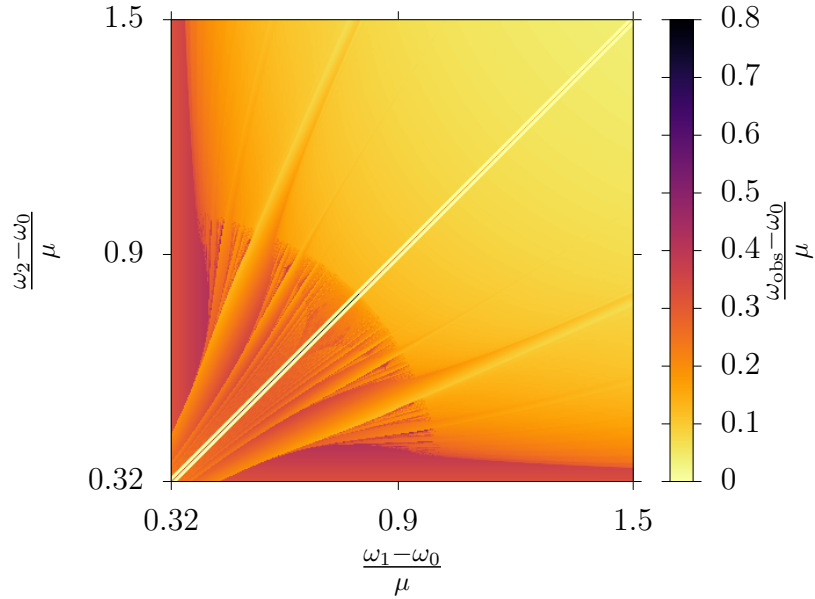
Figure 3.6: Focus on the region where both signals are outside the synchronization region. We observe synchronization to rational combinations of the two frequencies.

Variation of the parameters

To insure that the chosen parameters reflect a general behaviour of a van der Pol oscillator subject to a weak two-frequency signal we varied the parameter β, the phase θ, and the ratio of the amplitude of both frequencies. The corresponding results are illustrated in Fig. 3.7, Fig. 3.8, and Fig. 3.9 respectively. The variation of the phase only affects the behaviour on the diagonal line where both frequencies coincide. The variation of the parameter β scales the pattern of synchronization regions but does not influence the pattern itself much.
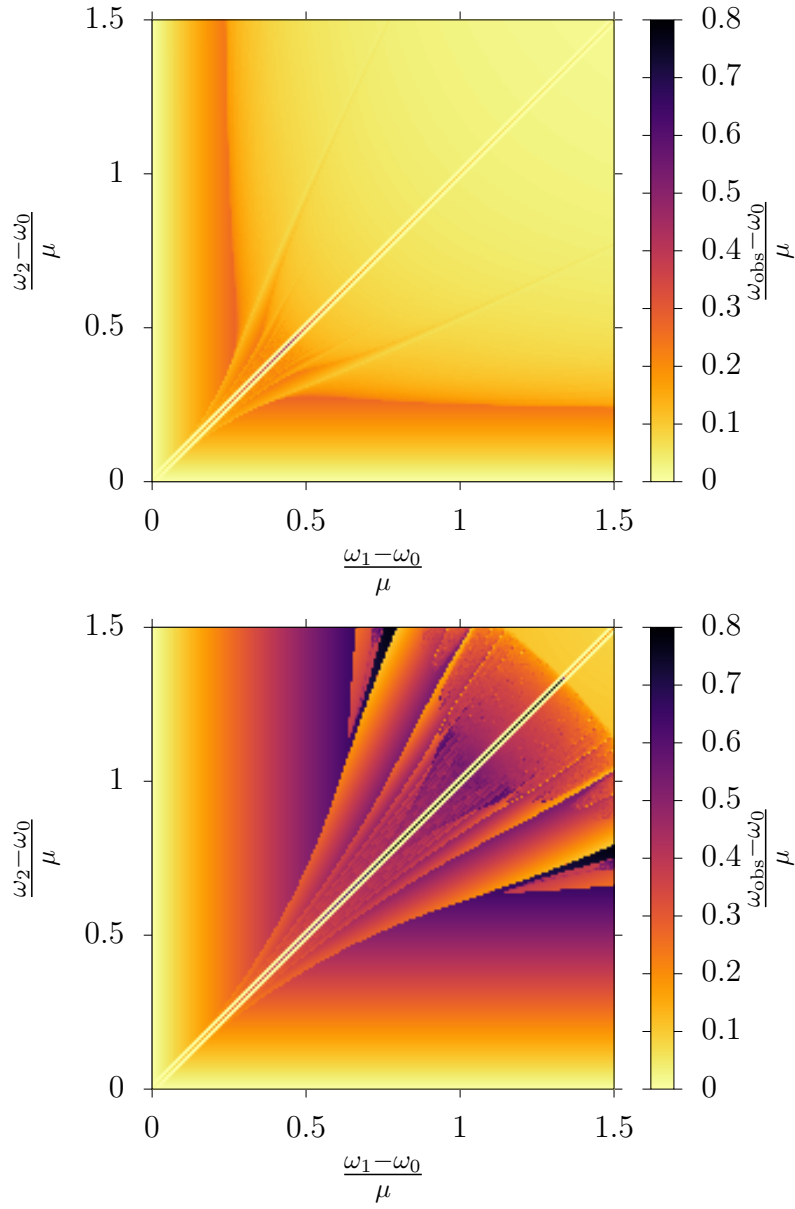
Figure 3.7: Variations of the parameter β. Upper graph $\beta = 0.2$, lower graph $\beta = 0.8$.
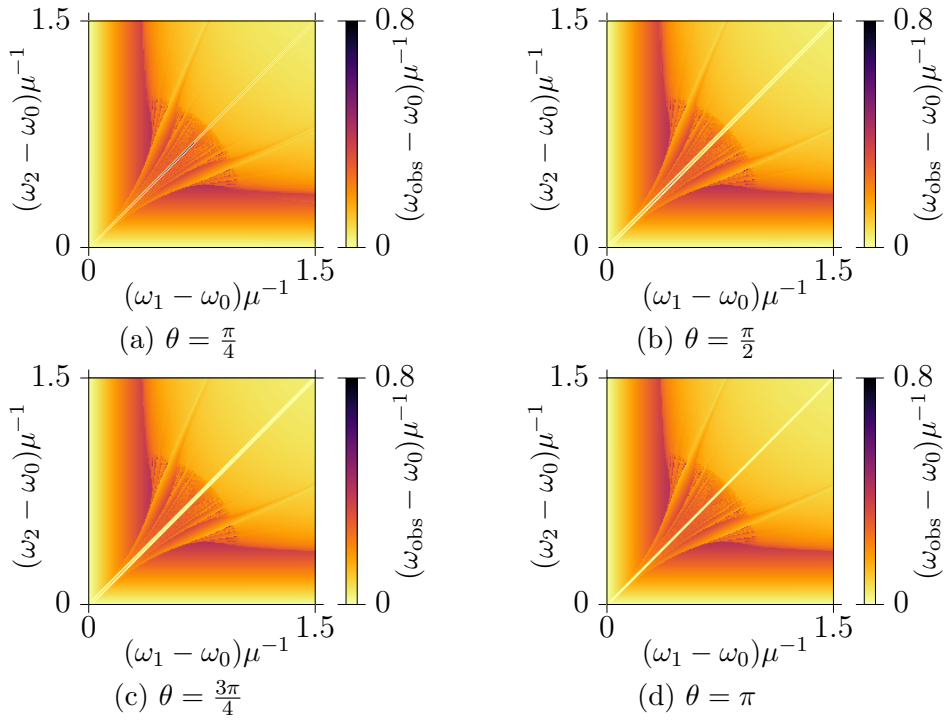
Figure 3.8: Different values of the phase
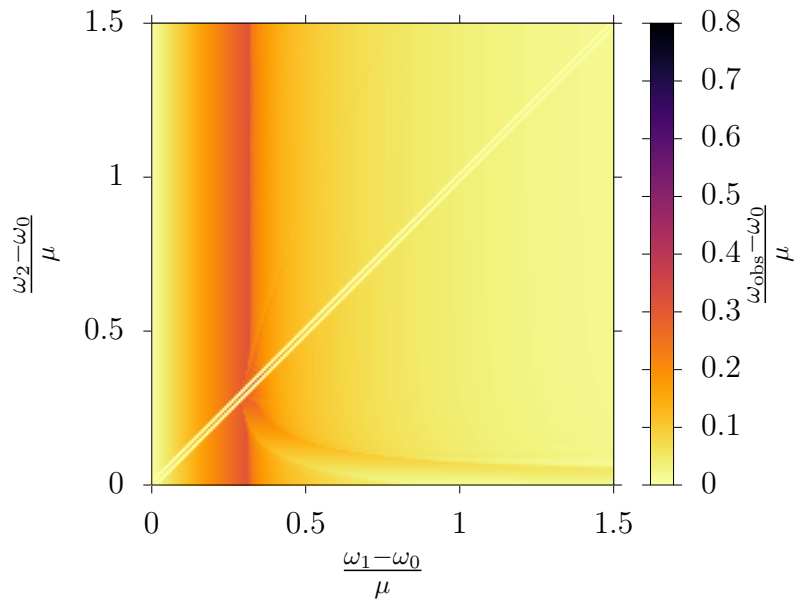
Figure 3.9: Change of the ratio between the amplitudes of the two signals K_1 and K_2. Here $K_1 = 2$ and $K_2 = 0.2$.

3.2 Simulation with noise

To find whether the pattern of synchronization regions persists under the influence of noise, we added a Gaussian white-noise term $\xi(t)$ to the phase of the van der Pol oscillator in the following way. For the numerical simulations, the differential equation (2.1) is rewritten into a system of first order differential equations,

$$\frac{\mathrm{d}}{\mathrm{dt}} \begin{pmatrix} u \\ \dot{u} \end{pmatrix} = \begin{pmatrix} \dot{u} \\ 2\epsilon\dot{u}(1 - \beta u^2) - \omega_0^2 u - \epsilon K_1 \cos(\omega_1 t) - \epsilon K_2 \cos(\omega_2 t + \theta) \end{pmatrix} \ . \tag{3.6}$$

To simulate a perturbation transversal to the limit cycle, we now added the noise term,

$$\vec{g} = \xi(t) \begin{pmatrix} -\dot{u} \\ u \end{pmatrix} \frac{1}{\sqrt{\dot{u}^2 + u^2}} \ , \tag{3.7}$$

to the system of equations (3.6). As can be expected from the theory of synchronization in the presence of noise [1], we observe a blurring of the synchronization borders. In the case of a single-frequency signal this is explained by an increased phase-slip rate due to the noise [1]. In the case of two frequencies, the same reasoning applies and is observed in Fig. 3.10a.
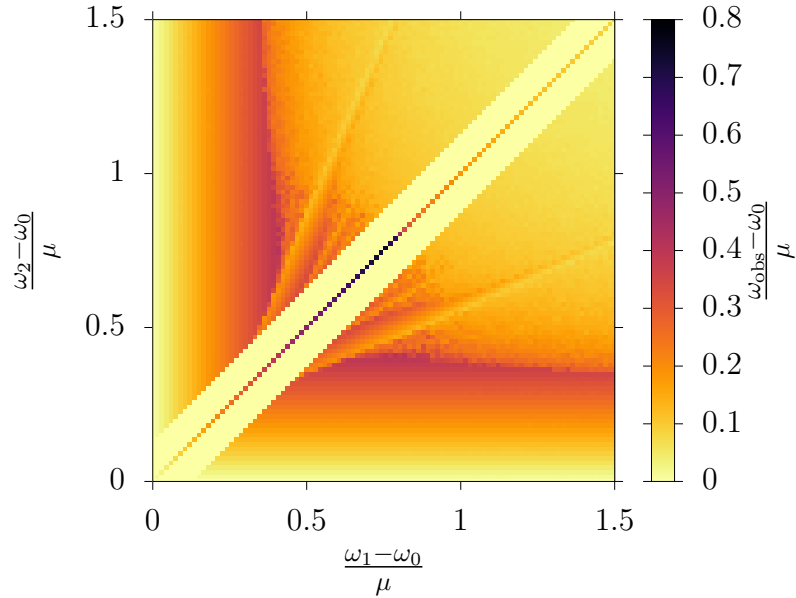
(a) Results of the simulation with the noise term Eq. (3.7) and a prefactor of 0.01, the same order of magnitude as the signal. The large bright yellow area around the diagnonal stems from a smaller timelimit we enforced due to the increased runtime of the stochastic differential equations solver.
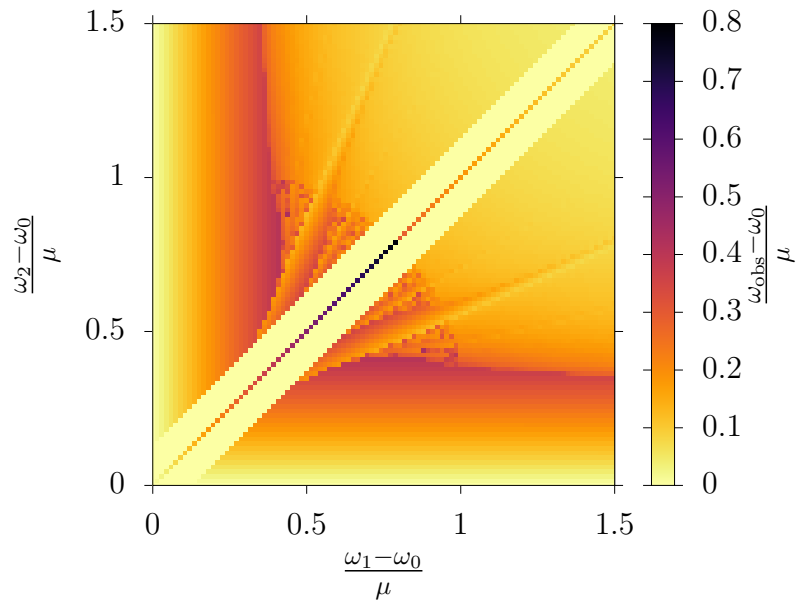
(b) Results of the simulation without the noise term.

Figure 3.10: Simulation (a) with and (b) without Gaussian white-noise term.

Conclusion

In this report we investigated the synchronization behaviour of a van der Pol oscillator subject to a two-frequency signal. We reviewed the theory of synchronization of a self-sustained oscillator to a periodic signal, and we detailed the knowledge on synchronization of such an oscillator to a signal containing two frequencies. We derived a system of differential equations to examine the synchronization of the oscillator in a rotating frame of adjustable frequency, Eqs. (2.13) & (2.12), and presented numerical evidence that the van der Pol oscillator indeed synchronizes to rational combinations of the frequencies. We discovered that synchronization regions for integer combinations of the drive frequencies show a higher stability and that their width decreases with the sum of the absolute values of the combinations.

We furthermore discovered that these patterns persist under the influence of Gaussian white noise of the order of the signal with the borders of the synchronization regions being blurred.

Further investigations could be made into the mechanism that amplifies the synchronization to one drive in the presence of another drive (region (b) in Fig. 3.2), the circular shape of the synchronization regions of combined frequencies, and the halo-like structure appearing in region (c) of Fig. 3.2 around the diagonal towards the end of the synchronization regions.

List of Symbols

χ General noise term

ν Dimensionless detuning

ϕ Phase of the solution in phase space

Ω Average velocity of the phase ϕ

ω_{border} Border of the synchronization region

ω_{obs} Observed frequency after a period of entrainment

ρ Rotation number

τ Dimensionless time

ξ Gaussian white-noise term in the numerical treatment

a Complex amplitude normalized to the natural amplitude

A Complex amplitude of the approximate solution

e Dimensionless drive strength

K Amplitude of the signal

p Prefactor of the second drive frequency in combination frequencies

q Prefactor of the first drive frequency in combination frequencies

ω_0 Natural frequency of the oscillator

ω_1 Frequency of the first signal

ω_2 Frequency of the second signal

θ_1 Constant phase shift of the first signal

θ_2 Constant phase shift of the second signal

K_1 Amplitude of the first signal

K_2 Amplitude of the second signal

u Amplitude of the signal

Appendices

Appendix A

Numerical Differentiation

To compute the gradient of our data we used the following approximation
for the derivative in x- and y-direction:

$$f'(x) \approx \frac{f(x+h) - f(x-h)}{2h} \ .$$

By expanding $f(x+h)$ and $f(x-h)$ one can show that this approximation
is exact up to second order. As h we took the step-size in the respective
direction.

Bibliography

[1] A. Pikovsky, M. Rosenblum, and J. Kurths, *Synchronization: A Universal Concept in Nonlinear Sciences.* Cambridge Nonlinear Science Series, (Cambridge University Press 2001).

[2] S. H. Strogatz, *Nonlinear Dynamics and Chaos*, (Perseus Books 1994).

[3] A. Pikovsky, M. Rosenblum, and J. Kurths, *Phase synchronization in regular and chaotic systems.* International Journal of Bifurcation and Chaos **10**(10), 2291 (2000).

[4] P. J. Holmes and D. A. Rand, *Bifurcations of the forced van der Pol oscillator.* Quarterly of Applied Mathematics **35**(4), 495 (1978).

[5] M. Ding, C. Grebogi, and E. Ott, *Evolution of attractors in quasiperiodically forced systems: From quasiperiodic to strange nonchaotic to chaotic.* Phys. Rev. A **39**, 2593 (1989).

[6] C. Gardiner, *Handbook of Stochastic Methods*, volume 13 of *Springer Series in Synergetics*, (Springer-Verlag Berlin Heidelberg 1997).

[7] C. Rackauckas and Q. Nie, *DifferentialEquations.jl - a performant and feature-rich ecosystem for solving differential equations in Julia.* Journal of Open Research Software **5**(1), 15 (2017).

[8] A. H. Nayfeh and P. D. T. Mook, *Nonlinear Oscillations*, (WILEY-VCH 1995).